National Conference with International Participation
ENGINEERING MECHANICS 2007
Svratka, Czech Republic, May 14 – 17, 2007

THERMOACOUSTICS

Z. Trávníček

Summary: *The thermoacoustic energy conversion systems can operate as heat pumps (or refrigerators which are based on the same principle) or prime movers. The design optimization of the thermoacoustic refrigerator was made using two methods, namely the optimization based on the cooling load maximization and on the coefficient of performance (COP) maximization. The highest COP can be achieved with the noble gas mixture helium-xenon (62%-38%) as the working fluid, while the highest cooling load can be achieved with pure helium.*

1. Introduction

The first powerful thermoacoustic refrigerators were designed in the USA (Hofler, 1986, Swift 1988, Garrett, 1991, Garrett *et al.,* 1993) in the late 1980's and early 1990's and the development continues there (e.g., Garrett, 2004). This initial research and development effort focused on the space applications, therefore the initial studies were connected with the world's leading laboratories such as the Los Alamos National Laboratories, NASA laboratories and several universities of the USA. Since the end of the last century, this field has been studied systematically by other teams (e.g., Wetzel and Herman, 1997 and 2000; Tijani *et al*., 2002a, b and c; Symko *et al.*, 2004; Herman and Trávníček, 2006). More recently several commercial companies are developing efficient thermoacoustic refrigerators for commercial applications such as the refrigerator for ice cream (Poese *et al.*, 2003) and thermoelectric power generator (Slaton and Zeegers, 2006). Despite that, the thermoacoustic field has received little interest in the Czech Republic.

The principle of thermoacoustic devices. The two types of the energy conversion devices are the prime movers (sometimes called "engine" – Swift 1988) and the heat pumps (or refrigerators, which are based on the same principle) as shown in Fig. 1. In a prime mover (Fig. 1a), heat flows through the device from high to low temperature, and the device generates work. Work can typically be converted to electric power. In a heat pump (Fig. 1b), the flows of heat and work are reversed: work is absorbed, and heat is extracted from a low-temperature source to a high-temperature sink. In *thermoacoustic* devices, the generated or absorbed mechanical work (via acoustic drivers or transducers, respectively) is work related to the acoustic field.

Fig. 2 shows a schematic model of the thermoacoustic refrigerator. Distributions of pressure, velocity and temperature within the half-wavelength resonance tube are indicated in Fig. 2b and 2c. The device consists of five basic parts: resonance tube, acoustic driver, and plate stack with cold and hot heat exchangers.

*Ing. Zdeněk Trávníček, CSc., Institute of Thermomechanics AS CR, Dolejškova 5, 182 00 Prague, Czech Republic; Phone: +420 266 053 305, Fax: +420 286 584 695; E-mail: tr@it.cas.cz

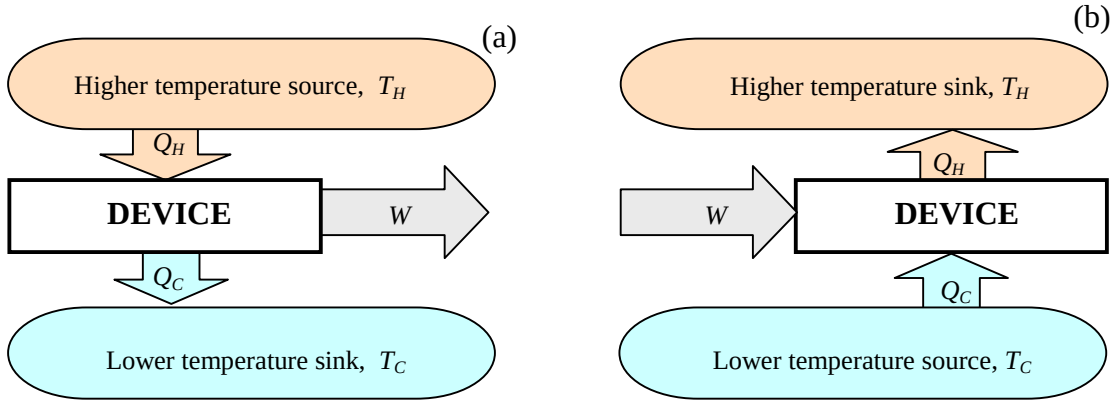

Fig. 1. Two types of energy conversion devices: (a) Prime mover: Q_H is heat flux from the higher temperature T_H, Q_C is heat flux to the lower temperature T_C, and W is the power output of the device. (b) Heat pump and refrigerator; Q_C is heat flux extracted from the lower temperature T_C, Q_H is heat flux to higher temperature T_H, and W is the power input of the device.

The principle of thermoacoustic heat transfer was described by the "fluid parcel model" (Swift, 1988; Wetzel and Herman, 1997). In Fig. 3a, the thermoacoustic effect is illustrated by considering the oscillation of a single gas parcel in the acoustic standing wave along the stack plate. The cycle contains two adiabatic steps (1 and 3) and two isobaric steps (2 and 4).

- Step 1: Due to the acoustic standing wave, the gas parcel moves left to an area of higher pressure and is adiabatically compressed as the ideal gas, thus the temperature increases.
- Step 2: The gas parcel is warmer than the stack plate and irreversible (isobaric) heat transfer from the gas parcel to the stack plate takes place.
- Step 3: After the acoustic wave has passed, the gas parcel moves right to its initial location, which has a lower pressure; during this adiabatic expansion temperature decreases.
- Step 4: The gas parcel is colder than the stack plate and irreversible isobaric heat transfer from the stack plate towards the gas parcel takes place.

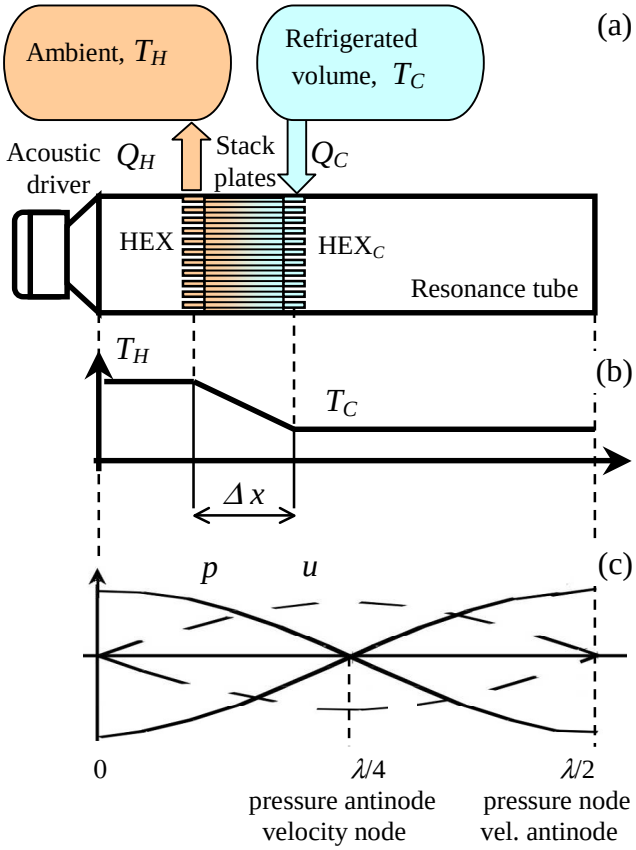

Fig. 2. Schematic of the thermoacoustic refrigerator. (a) Resonance tube; HEX_C and HEX_H are the cold and hot heat exchangers, respectively. (b) Temperature, (c) pressure and velocity distribution along the half-wavelength resonance tube.

At this time, the gas parcel has returned to its initial pressure, temperature and position and the cycle starts over again. Since there are many gas parcels moving along the stack plate, heat is dropped by one gas parcel, and transported further by the adjacent parcel; the pattern was metaphorically called a “bucket-brigade” by Swift, 1988 (Fig. 3b). This cyclic movement creates a temperature gradient along the stack plate.

The thermoacoustic cycle described above is identical to the reverse Brayton cycle, which is presented in Fig. 3c. Obviously, the thermoacoustic refrigerator could not function if the steps of irreversible heat transfer ((2) and (4) in Fig. 3a) were removed. Therefore, the thermoacoustic refrigerator has to be designed to maximize the intrinsic irreversibilities.

For comparison, vapor compression refrigeration is based on the Rankine cycle, which exploits a liquid-gas phase change and has intrinsic irreversibilities in the free expansion and cooling of the gas phase (in order to improve the performance of the Rankine cycle of the classic vapor compression refrigerators, the effect of irreversibilities within the thermodynamic cycle has to be minimized).

First and second laws of thermodynamics for one cycle the system. The balance of energy fluxes is determined by the first law of thermodynamics as

$$Q_H = Q_C + W, \qquad (1)$$

where Q_C is heat flux extracted from the lower temperature T_C, Q_H is heat flux transferred to higher temperature T_H, and W is the power input of the device.

The efficiency of energy conversion devices is expressed as the desired output divided by the required input. For the heat pump and refrigerator, the efficiency is called the *coefficient of performance* COP = Q_C / W.

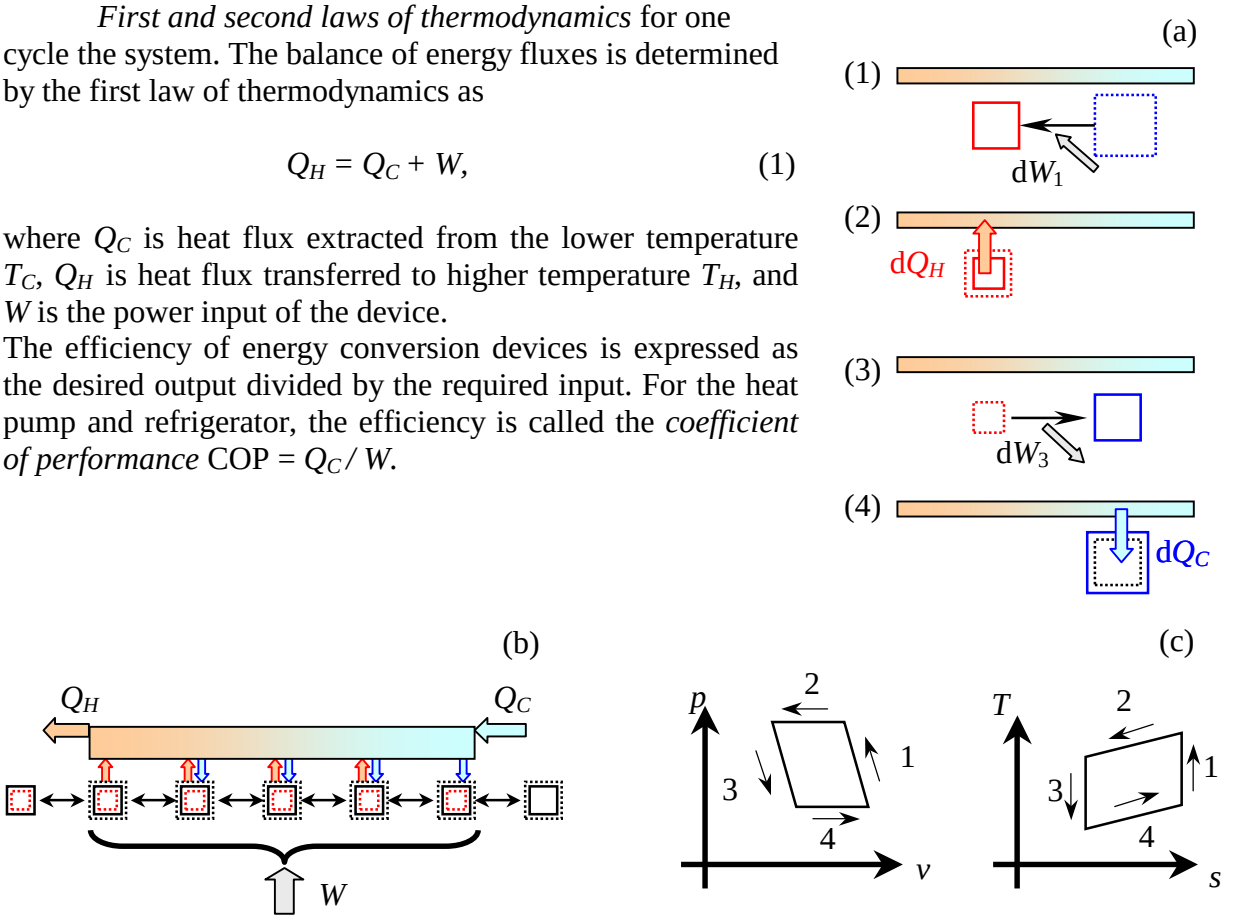

Fig. 3. Illustration of the thermoacoustic cycle of the typical oscillating gas parcel. (a) four steps of the cycle (initial and final states of the oscillated gas parcel are plotted using dotted and solid lines, respectively): (1) adiabatic compression, (2) irreversible isobaric heat transfer from the gas parcel to the stack plate, (3) adiabatic expansion, and (4) irreversible isobaric heat transfer towards the gas parcel. (b) Resultant heat transport along the stack plate via a chain of fluid parcels – the so called “bucket brigade”(Swift, 1988). (c) Thermoacoustic (reverse Brayton) cycle 1–4 of Fig. 3a in p–V and T–s diagrams.

The second law of thermodynamics at integration states

$$Q_H/T_H = Q_C/T_C + S_i \tag{2}$$

where S_i is the irreversible entropy production in the system. Since the entropy generation must be positive or zero $S_i \geq 0$, Eq. (2) gives

$$Q_C/T_C \leq Q_H/T_H \tag{3}$$

and Eqs. (1 and 2) give COP $\leq T_C/(T_H - T_C)$.
The temperature ratio on the right hand side of Eq.(3) is called the Carnot's coefficient of performance, $COP_C = T_C/(T_H - T_C)$; it is the maximal COP that a heat pump and refrigerator can achieve. In other words, the second law limits the COP as COP $\leq COP_C$. The coefficient of performance relative to Carnot's coefficient is defined as COPR = COP/COP_C:

$$COPR = \frac{Q_C (T_H - T_C)}{W T_C} \tag{4}$$

2. Parameters

The dimensions are defined by resonance tube length L (this paper deals with a half wavelength resonance tube, thus $L = \lambda/2$), diameter D, stack plate length Δx, and stack center location x_C. In nondimensional form, stack length ξ and stack center position ξ_C can be expressed (Wetzel and Herman, 1997) as $\xi = \frac{2\pi\Delta x}{\lambda}$, $\xi_C = \frac{2\pi x_C}{\lambda}$, respectively.
Inverse normalized plate spacing is the ratio of the thermal penetration depth to plate spacing h: $\delta_{\kappa h} = \delta_\kappa / h$. The relative free cross section (blockage ratio) BR is the ration of the stack plate thickness t and stack plate spacing h: $BR = h/(h+t)$.

Stack material parameters are expressed by the stack heat capacity correction factor:

$$\varepsilon_s = \sqrt{\frac{\rho_m c_p K}{\rho_S c_S K_S}} \tag{5}$$

where ρ, c, and K are density, isobaric heat capacity, and thermal conductivity, respectively (index s means stack material).

Two characteristic length scales of the thermoacoustic core the thermal penetration depth δ_κ (the thickness of the layer where the thermoacoustic effect occurs) and the viscous penetration depth δ_ν (the thickness of the layer that is restrained in movement under the influence of viscous forces):

$$\delta_\kappa \equiv \sqrt{2\alpha/\omega} \tag{6}$$

$$\delta_\nu \equiv \sqrt{2\nu/\omega} \tag{7}$$

where α and ν are thermal diffusivity and kinematic viscosity (momentum diffusivity) of the working fluid, respectively, and ω is the angular frequency. In the calculation of α ($\alpha = k/c_p \rho$), k, c_p and ρ are thermal conductivity, isobaric heat capacity, and density of the working fluid, respectively.

Heat and work fluxes (Q_C and W) were derived for the short stack boundary layer approximation by Swift, 1988. Using the nondimensional adaptation by Wetzel and Herman, 1997, heat flux Q_H, work flux W, and cooling load Q_C can be expressed as

$$Q_H = A\, p_m\, c\, \Phi_H \tag{8}$$

$$W = A\, p_m\, c\, \Phi_W \tag{9}$$

where A is the stack cross sectional area, p_m is the mean pressure of the working fluid, c is the sound speed in the working fluid, and the nondimensional heat and work fluxes were derived by Wetzel and Herman, 1997 as

$$\Phi_H = \frac{-\delta_{\kappa h}\, DR^2}{2\gamma} \; \frac{\cos(\xi_c)\sin(\xi_c)}{(1+Pr)(1+\varepsilon_s)(1-2Pr^{1/2}\delta_{\kappa h}+2Pr\,\delta_{\kappa h}{}^2)} \times \left[\frac{1+Pr^{1/2}+Pr\,(1+\varepsilon_s)}{1+Pr^{1/2}}\frac{\xi_{crit}(\theta)}{\xi} - (1+Pr^{1/2}\cdot(1-2\cdot\delta_{\kappa h}))\right] \tag{10}$$

$$\Phi_W = \frac{\delta_{\kappa h}\, DR^2}{2\,\gamma} \left[\frac{BR\,(\gamma-1)\cos^2(\xi_c)}{(1+Pr^{1/2})\,(1+\varepsilon_s)\,(1-2Pr^{1/2}\,\delta_{\kappa h}+2Pr\,\delta_{\kappa h}{}^2)}\,\xi_{crit}(\theta) - \left(\frac{BR\,(\gamma-1)\cos^2(\xi_c)}{1+\varepsilon_s} + \frac{Pr^{1/2}\sin^2(\xi_c)}{BR\,(1-2\,\mathrm{Pr}^{1/2}\,\delta_{\kappa h}+2Pr\,\delta_{\kappa h}{}^2)}\right)\xi \right] \tag{11}$$

where DR is the ratio of the pressure amplitude at the pressure antinode of the standing wave P_A to the mean pressure of the working fluid p_m ($DR = P_A/p_m$), γ is the ratio of the isobaric to isochoric specific heats for the working fluid, Pr is the working fluid's Prandtl number, θ is the normalized temperature difference ($\theta = \Delta T/T_m = (T_H - T_C)/T_m$), T_m is the mean temperature, ($T_m = T_H + T_C$)/2, and ξ_{crit} is the nondimensional critical stack length, $\xi_{crit} \equiv \dfrac{\theta}{BR(\gamma-1)\cot(\xi_c)}$.

Taking into account the first law of thermodynamics, and proportionality $c \sim T_m^{0.5}$, cooling load can be expressed as the functional dependence

$$Q_C = (\pi/4)\, D^2\, p_m\, DR^2\, T_m^{0.5}\, F(Pr,\ \gamma,\ \varepsilon_s,\ \theta,\ \xi,\ \xi_C,\ BR,\ \delta_{kh}) \tag{12}$$

where the function $F(Pr,\ \gamma,\ \varepsilon_s,\ \theta,\ \xi,\ \xi_C,\ BR,\ \delta_{kh})$ depends on eight non-dimensional parameters

$$F(Pr,\ \gamma,\ \varepsilon_s,\ \theta,\ \xi,\ \xi_C,\ BR,\ \delta_{kh}) = (\Phi_H - \Phi_W)\frac{\sqrt{R\gamma}}{DR^2}, \tag{13}$$

where R is the specific gas constant.

3. Results and discussion: Design optimization and performance calculation

Thermal devices and their theory, design and research, involve a range of engineering applications and tasks. Two types of tasks are design problems and performance calculations. The first task, the *design problem* (or *sizing problem*) deals with the design of a new device for a specific set of input and output conditions consisting of thermo physical and material parameters and geometry constraints. The second task, the *performance calculation*, predicts the output conditions including and heat transfer rate for the existing device with a specific set of input parameters.

The choice of the optimization method and its criteria depends on the specific character of the device, required function, and design constraints. An effective design of heat transfer equipment typically uses one of the classical optimization methods (Eckert, Drake, 1950; Bejan, 1995, Bejan, 1982, Bejan *et al*., 1996, and Bejan *et al*., 2000).

The COP and COPR play an important role in the design of the thermoacoustic refrigerator. On the other hand, COP and COPR are relative parameters, which have to be used with a reasonable caution. The reason is that a device with a relatively high COP and COPR (both are desirable) can give an insignificantly small cooling load (because the

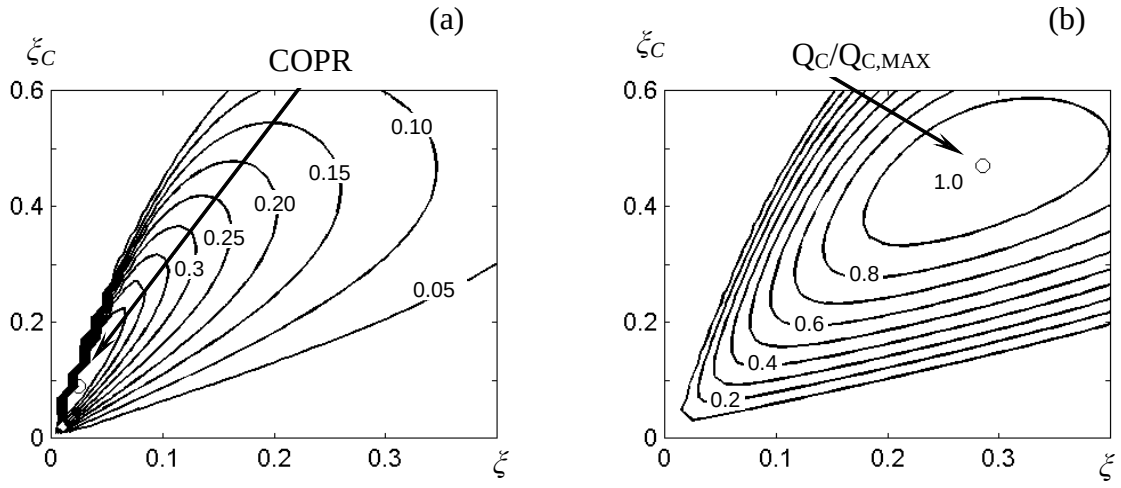

Fig. 4 Performance of the thermoacoustic refrigerator with He-Xe (89%/11%) mixture as a function of the stack center position ξ_C and the stack length ξ.

maximum COP and Q_C do not coincide – Herman, Trávníček, 2006). Hence the cooling load Q_C can be chosen as the *absolute* optimization criterion by means of the Q_C maximization (Minner et al, 1995; Herman, Trávníček, 2006).

Input parameters of the design optimization are the design requirements (T_H and T_C temperatures, mean pressure and drive ratio), material and geometry specific parameters. Fig. 4a and 4b show contour lines representing functions COPR(ξ_C, ξ) and $Q_C(\xi_C, \xi)$ for the specific parameters, which are very close to the parameters of the "Thermoacoustic Life Science Refrigerator" (TALSR) designed by Garrett, 1991: A noble gas mixture Helium–Xenon, 89%–11% (i.e. Pr = 0.27, c = 1.67 and c = 456.6 m/s –see Giacobbe, 1994; Belcher *et al.*, 1999), material of the stack is Mylar^{TM} (i.e. ε_S=0.47), $L = \lambda/2$ = 950 mm, D=110 mm, p_m = 2 10^6 Pa, $DR = P_A/p_m$ 3.5%, T_C=260.25K, T_H= 285.75K, $BR= h/(h+t)$ =0.80, and $\delta_{kh} = \delta_\kappa / h$ = 0.414, (i.e. $T_m=(T_H+T_C)/2$=273.00K, $\theta = \Delta T/ T_m=(T_H-T_C)/T_m$ = 0.093, COPc= $T_C/(T_H-T_C)$ = 10.21).

Design optimization for best COPR: In order to quantitatively visualize the location of the optimal ξ_C and ξ, Figs. 4a was plotted as a 2D graph with contour lines representing values of constant COPR. Fig. 4a shows that the optimal ξ_C, ξ pair exists for maximum COPR relatively close to the coordinate's origin: $COPR_{MAX}$= 0.58 for ξ_C = 0.090 and ξ = 0.025.

Design optimization for best cooling load: In contrast to the maximum COPR, the maximum of the function $Q_C(\xi_C, \xi)$ is located far away from the origin, as shown in Fig. 6d: $Q_{C,MAX}$ = 238.2W for ξ_C = 0.470 and ξ = 0.285 (Fig. 4b).

Performance calculation: The performance of the optimal thermoacoustic refrigerators expressed in terms of the COPR, Φ_C and Q_C as a function of stack length for the selected working fluids (*working fluid effect***)** is shown in Fig. 5. The parameters were $L=\lambda/2$=950 mm, D=110 mm, p_m =2 10^6 Pa, $DR=P_A/p_m$ 3.5%, T_C=260.25K, T_H=285.75K, $BR=h/(h+t)$=0.80, and $\delta_{kh} = \delta_\kappa/h$ = 0.414, (i.e. T_m= $(T_H+T_C)/2$=273.00K, $\theta = \Delta T/ T_m=(T_H - T_C)/T_m$ = 0.093, COPc= $T_C/(T_H-T_C)$ = 10.21).

Four working fluids were considered using the optimized stack center position (to achieve the maximum Q_C): Air (Pr = 0.71, $\xi_{C,OPT}$ = 0.29), Helium (Pr = 0.67, $\xi_{C,OPT}$ = 0.33), He–Xe, 89%–11%, (Pr = 0.27, $\xi_{C,OPT}$ = 0.47), and He–Xe, 62%-38% (Pr = 0.18, $\xi_{C,OPT}$ = 0.51).

Fig. 5a shows that decreasing *Pr* increases the COPR. The reason is that decreasing *Pr* increases the difference between the thermal and viscous penetration depths. Therefore decreasing *Pr* contributes positively to the thermoacoustic effect, thus it increases the efficiency (COP and COPR) of the thermoacoustic core. The thermoacoustic refrigerator with the He–Xe(62%–38%), i.e. Pr = 0.18 gives the highest $COPR_{MAX}$ = 0.232 for ξ_C = 0.51 and ξ = 0.17 (at Q_C = 144.8W). As expected, the smallest COPR value is achieved by using air as the working fluid (on the other hand, air is a very cheap working fluid, recommendable for testing purposes). Fig. 5b shows that the influence of the *Pr* on the non-dimensional cooling load Φ_C is similar to its influence on the COPR: The *Pr* decrease causes an increase of the Φ_C.

In contrast with the COPR–*Pr* and Φ_C –*Pr* relationships in Figs. 5a and 5b, respectively, small values of *Pr* don't render a high cooling load automatically as shown in Fig. 5c. Despite the fact the *Pr* number of the gas mixture He-Xe 62%-38% is the smallest of all (*Pr* = 0.18), it causes very small Q_C: the cooling load with pure Helium is 2 times higher than using the He-Xe

(62%-38%) mixture (!) The thermoacoustic refrigerator with pure Helium gives the highest cooling load of all noble gases and their mixtures: $Q_{C,MAX}$ = 324.8W for ξ_C = 0.33 and ξ = 0.215 (at COPR= 0.108).

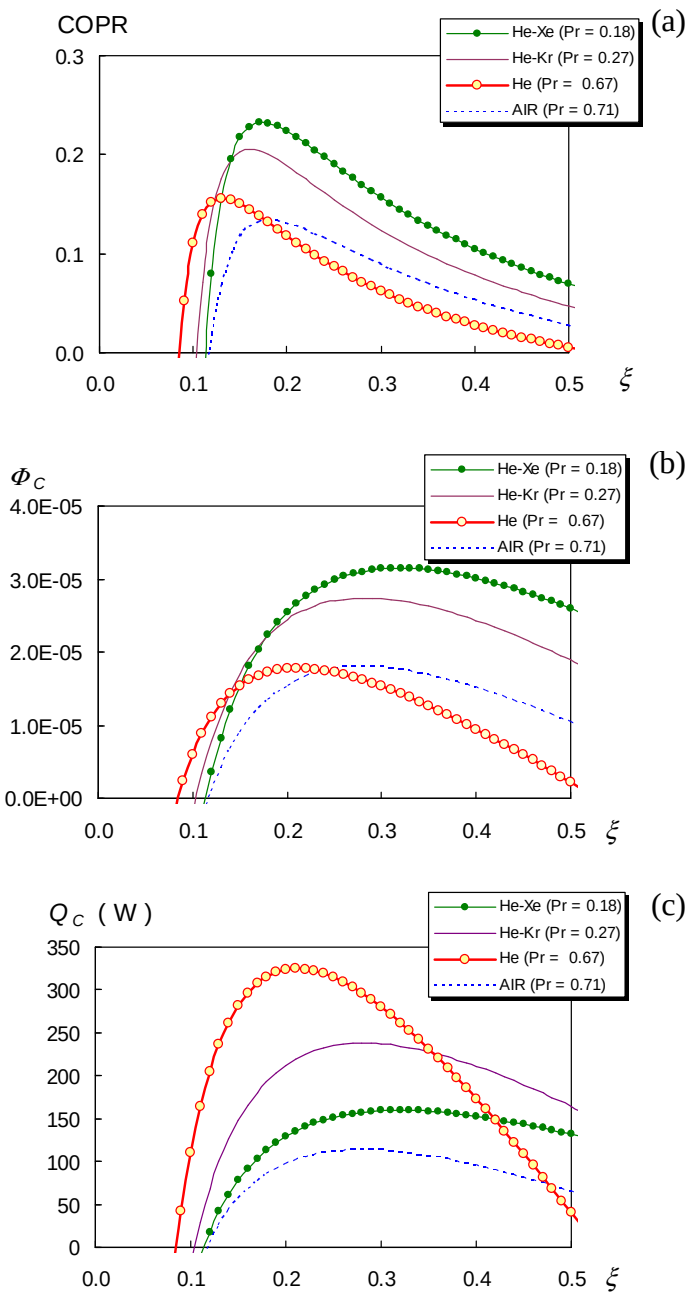

Fig. 5. Performance of the thermoacoustic refrigerators for various working fluids at optimal stack center position (ξ_C=0.29–0.51 depending on the fluid), as a function of the stack length ξ, expressed through (a) COPR, (b) Φ_C and (c) Q_C.

The dependence of Q_C and COPR on stack length for various working fluids is shown in Fig. 6. The parameters for this calculation are the same as for Fig. 5, i.e. each of the curves was plotted for the optimal stack center position ξ_C, which was determined for each of the working fluids. For small ξ, the COPR as well as Q_C is small, implying that the stack plates are "too short". The smallest value of ξ is at the graph origin, and represents the critical stack length for the onset of the thermoacoustic effect (Wetzel and Herman, 1997). An increase of the ξ causes the *COPR* as well as Q_C to increase.

For example of Helium, the maximum COPR is achieved at ξ = 0.13 ($COPR_{MAX}$ = 0.155 and Q_C = 236.8W) and the maximum Q_C is achieved at ξ = 0.215 ($Q_{C,MAX}$ = 324.8W and COPR = 0.108). Increasing ξ past the length for optimal COPR or Q_C causes COPR or Q_C to decrease, which indicates that the stack is "too long".

Temperature and pressure effect: The effect of varying T_m in a the optimal thermoacoustic refrigerator with Helium is shown in Fig. 7. The parameters for this calculation are the same as for Figs. 5 and 6, (Helium with $\xi_{C,OPT}$=0.33, ξ_{OPT} = 0.215**)**, corresponding to the maximum Q_C. Fig. 7 shows that COPR is independent of T_m. The COPR – Q_C relationship has the maximum, which is located at approximately θ = 0.12, (i.e., at COP_C = 8.0).

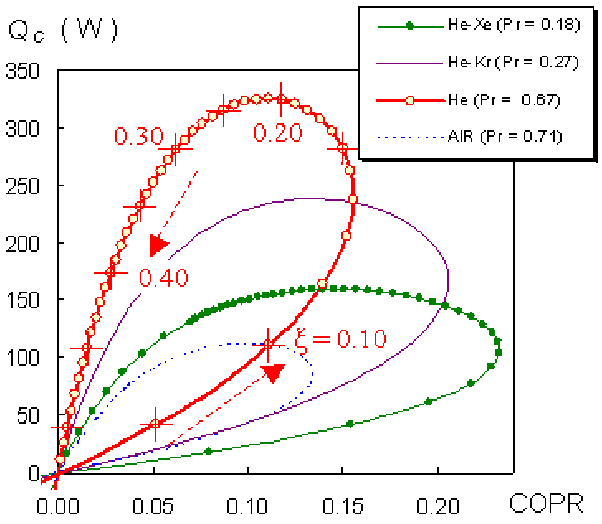

Fig. 6. Performance of the thermoacoustic refrigerators as a function of the stack length ξ expressed through the cooling load Q_C and COPR. The stack length ξ increases counter clockwise along the curves, as indicated for Helium by the arrows.

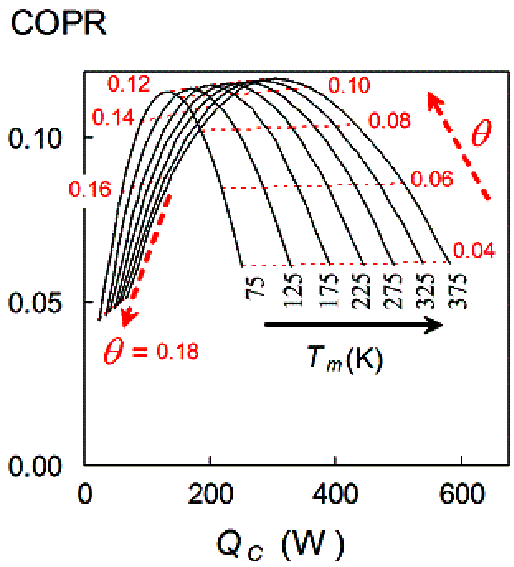

Fig. 7. Performance of the optimal thermoacoustic refrigerator with Helium as the working fluid.

Fig. 7 shows that Q_C increases with the T_m. The reason is that Q_C is proportional to the sound speed, which is, for ideal gases, proportional to the $T_m^{0.5}$. Therefore the cooling load Q_C is practically proportional to the $T_m^{0.5}$. The Q_C decreases when θ increases; the limit of the θ increase is related with the maximum temperature difference on the stack, when the cooling load is zero and the thermoacoustic function ends (Wetzel and Herman, 1997).

The effect of pressure can be explained by considering Eq.(12): Thermoacoustic refrigerator cooling load is proportional to the p_m. This effect is slightly reduces by the temperature influence on material properties of fluids. For example, the pressure increase by the factor of five causes the Q_C increase by the factor 4.8 or 4.9 in Helium or air, respectively.

4. Conclusion

The thermoacoustic energy conversion systems can operate as heat pumps (or refrigerators) or prime movers. The design optimization of the thermoacoustic refrigerator was made using two methods, namely the optimization based on the cooling load maximization and the optimization based on the COP maximization. It was shown that the results of these methods do not coincide. The performance calculation for various working fluids demonstrates that the highest COPR can be achieved with the noble gas mixture He–Xe (62%–38%, i.e. Pr = 0.18) as the working fluid. On the other hand, the highest cooling load can be achieved with pure Helium.

The advantage of the thermoacoustic devices is that their only moving part is the acoustic actuator. This results in increased reliability of the equipment. Noble gases and their

mixtures are typically used as the working fluid. Therefore, the thermoacoustic devices are an attractive technological solution from the environmental perspective because they do not rely on hazardous refrigerants. The potential of thermoacoustic processes can be utilized to improve the design of industrial devices such as heat pumps, refrigerators, pulsating burners, and mixture separators. Thermoacoustics is a promising field for various applications such as food processing industry, automotive and chemical engineering, etc.

5. Acknowledgement

I gratefully acknowledge the support by the Grant Agency of the Czech Republic (project No. 101/05/2681).

6. References

Bejan A. (1977) The concept of irreversibility in heat exchanger design: Counterflow heat exchangers for gas-gas applications. *J Heat Transfer Trans*, 99, pp.374-380

Bejan A. (1982) Entropy generation through heat and fluid flow. John Wiley & Sons, New York.

Bejan A. (1995) Convection Heat Transfer. John Wiley & Sons, Inc., New York.

Bejan A., Tsatsaronis G., Moran M. (1996) Thermal design and optimization. Wiley, New York.

Bejan A., Rocha L.A.O., Lorente S. (2000) Thermodynamic optimization of geometry: T- and Y- shaped constructs of fluid streams. *Int J Therm Sci*, 39, pp.949-960.

Belcher J.R. *et al.* (1999) Working gases in thermoacoustic engines. *J Acoust Soc Am*, 105, pp.2677-2684.

Eckert E.R.G., Drake R.M. (1950) Introduction to the transfer of heat and Mass. McGraw-Hill, New York.

Garrett S.L. (1991) Thermoacoustic Life Science Refrigerator, NASA Tech. Report No. LS-10114. Johnson Space Center, Houston, TX.

Garrett S.L., Adeff J.A., Hofler T.J. (1993) Thermoacoustic refrigerator for space applications. *J Thermophys and Heat Trans,* 7, pp.595-599.

Garrett S.L. (2004) Resource letter: TA-1: Thermoacoustic engines and refrigerators. Am J Phys, 72, (1), pp.11-17.

Giacobbe F.W. (1994) Estimation of Prandtl numbers in binary mixtures of helium and other noble gases. *J Acoust Soc Am*, 96, pp.3568-3580.

Herman C., Trávníček Z. (2006) Cool sound: The future of refrigeration? Thermodynamic and heat transfer issues in thermoacoustic refrigeration. *Heat and Mass Transfer*, 42, (6) pp.492-500.

Hofler T.J. (1986) Thermoacoustic refrigerator design and performance, Ph.D. Dissertation, University of California, San Diego.

Kirchhoff G. (1868) Über den Einfluss der Wärmeleitung in einem Gase auf die Schallbewegung. *Ann Phys*, 210, pp.177-193.

Minner B.L., Mongeau L., Braun J.E. (1995) Optimization of thermoacoustic engine design variables for maximum performance. *J Acoust Soc Am,* 98, 2961-2962.

Poese E.P., Smith R.W.M., and Garrett S.L. (2003) Regenerator-based thermoacoustic refrigerator for ice cream storage applications. *J Acoust Soc Am,* 114, (4) pp.2328-2328.

Rott N. (1980) Thermoacoustics. *Adv Apl Mech,* 20, pp.135-175.

Slaton W.V., Zeegers J.C.H. (2006) Thermoelectric power generation in a thermoacoustic refrigerator. *Appl Acoust,* 67, (5), pp.450-460.

Symko O.G., Abdel-Rahman E., Kwon Y.S., *et al.* (2004) Design and development of high-frequency thermoacoustic engines for thermal management in microelectronics. *Microelectron J,* 35, (2) pp.185-191.

Swift G.W. (1988) Thermoacoustic engines. J Acoust. Soc Am, 84, pp.1145-1180.

Tijani M.E.H., Zeegers J.C.H., de Waele A.T.A.M. (2002a) Construction and performance of a thermoacoustic refrigerator. *Cryogenics,* 42, pp.59-66.

Tijani M.E.H., Zeegers J.C.H., de Waele A.T.A.M. (2002b) Design of thermoacoustic refrigerators. *Cryogenics,* 42, (1) pp.49-57.

Tijani M.E.H., Zeegers J.C.H., de Waele A.T.A.M. (2002c) The optimal stack spacing for thermoacoustic refrigeration. *J Acoust Soc Am,* 112, pp.128-133.

Wetzel M, Herman C (1997) Design optimization of thermoacoustic refrigerators. *Int J Refrig,* 20, pp.3-21.

Wetzel M, Herman C, (2000) Experimental study of thermoacoustic effect on single plate Part I: Temperature fields. *Heat and Mass Transfer,* 36, pp.7-20.

Wheatley JC, Hofler T, Swift GW, Migliori A (1983) An intrinsically irreversible thermoacoustic heat engine. *J Acoust Soc Am,* 74, pp.153-170.